Article

Selective Gamma-Ray Ionisation of Vanadium Oxides: Towards the Formation of VO_2

M. Ndiaye[1]
https://orcid.org/0000-0001-7712-419X
pap822008@yahoo.fr

O. Sakh[1]
https://orcid.org/0000-0002-0629-1713

A. Seck[1,2]
https://orcid.org/0000-0003-3339-0933

B. D. Ngom[1]
https://orcid.org/0000-0002-5362-9211

M. Maaza[3,4]
https://orcid.org/0000-0002-3820-7838

M. Chaker[2]
https://orcid.org/0000-0001-9781-8842

Abstract

In this study, we report on the valence control of vanadium oxidation states towards stabilising VO_2 thin films. X-ray diffraction measurements indicate that up to 300 kGy of gamma-ray radiation the VO_2 phase remains monoclinic, with the crystallite size only varying slightly with the dose. X-ray photoemission spectroscopy indicates the presence of three oxide phases (VO_2, V_2O_3 and V_2O_5) on the samples. A decrease in the oxidation states of V^{3+} and V^{5+} and an increase in the valence state V^{4+} are observed for irradiations up to 300 kGy, which favours the vanadium dioxide VO_2 formation.

Keywords: vanadium oxides; gamma-ray irradiation; structural properties; CubeSats; thermal shielding

1 Quantum Photonics, Energies and Nanofabrication Laboratory, Faculty of Science and Technology, Cheikh Anta Diop University of Dakar, Senegal.
2 National Institute for Scientific Research, Energy and Materials, Canada.
3 UNESCO–UNISA Africa Chair in Nanoscience and Nanotechnology, College of Graduate Studies, University of South Africa.
4 Nanosciences African Network iThemba LABS-National Research Foundation, South Africa.

UNISA university of south africa PRESS
Nano-Horizons
Volume 2 | 2023 | 20 pages

Nano-Horizons
https://doi.org/10.25159/3005-2602/14875
ISSN 3005-2602 (Online)

1 Introduction

Vanadium dioxide (VO_2) is classified as a smart material, ie a material that exhibits changes in properties (such as electrical, optical and magnetic properties) when subjected to external stimuli. Vanadium dioxide can be obtained in different forms: solid forms [1], thin films [2], [3], nanowires [4], nanoparticles [5], and other nanostructures [6], [7]. Vanadium dioxide exhibits exciting properties owing to its insulator-to-metal transition, accompanied by structural and optical changes at near room temperature (insulator-to-metal transition temperature ITMT ~ 341 K) [8], [9]. The transformation of its crystallographic structure from monoclinic at temperatures below TTIM to tetragonal at temperatures above TTIM is ultrafast (less than one picosecond) and reversible [10]. The magnitude of the electrical (electrical resistivity) and optical (optical transmission) transitions depends on the microstructure and electronic properties of the material [11], [12]. Many applications are possible for (VO_2) such as electrical switches, smart windows, and gas detectors [10]. Owing to these properties and the vast potential of (VO_2) for applications, including smart radiators and as a thermal protective coating to limit radiation on sensitive opt electrical devices in spacecraft [13], [14], it is useful to investigate different ways of stabilising VO_2.

Much heat exchange between an object in space and the environment is carried out by radiation. These radiations include charged particles such as electrons (beta particles β), protons (p), alphas (α), ions from fission fragments, and neutral radiation, including photons (gamma and X-rays). The behaviour of charged particles (α, β, p) passing through matter is fundamentally different from that of neutral radiation (n, γ). Charged particles in particular interact strongly with the orbital electrons of the material through which the particles travel. When solids are bombarded by radiation, electrons can be removed from their orbits and atoms can be driven from their sites. In addition, impurities can be introduced by nuclear transmutation or bombarding ions implanted in the material. As a result, irradiated solids can have their properties modified either slightly or radically [15]–[20].

Studies on the irradiation of (VO_2) thin films with heavy ions [20]–[24] have indicated that displacement cascades occur, which is the driving mechanism by which disordered regions and defects are homogeneously generated in thin films [25]. These studies have also indicated that irradiation-induced defects change the phase transition temperature of (VO_2) by lowering both the phase transition temperature and most semiconductor phases. Recent studies on atom displacement by gamma rays report that measurable defects can be produced [26]. By subjecting the material to fast neutrons, the majority of the displaced atoms result from the collisions caused by the direct strikes during the quiescent deceleration. Bombardment of materials by fast neutrons has been reported to induce irregularities and alterations in the lattice structure, affecting the chemical and electrical properties [15], [27]–[29]. At high energy (± 1.5 MeV), Compton scattering and production of electron-hole pairs are believed to be likely the interaction processes leading to atomic displacement or collision damage in materials.

In this work, we propose to investigate the effects of gamma-ray irradiation on the crystal and electronic structure of (VO_2) thin films. This study is relevant for determining the space applicability in CubeSats.

2 Experimental Details

The (VO_2) thin films were deposited using pulsed laser deposition on a soda glass substrate maintained at a temperature of 600 °C for a deposition time of 45 min. A krypton fluoride excimer laser with a wavelength of 248 nm at a fluence of 1.7 J/cm^2 and a repetition rate of 10 Hz was used to irradiate the vanadium metal target. The deposition was carried out in an oxygen atmosphere at 2.00 Pa. The resulting thickness of the film is equal to 80 nm. This sample was split into four samples subjected to 0, 50, 100 and 300 kGy gamma-ray radiations, respectively. A cobalt-60 panoramic point source irradiator (ARC Infruitec Stellenbosch, Western Cape, South Africa) irradiated the samples. The samples were mounted on a turntable at 250 mm from the source for the irradiation experiments. The turntable, perpendicular to the source, rotates around the Z-axis at 2 rpm for the irradiation duration.

Dose rate measurements were performed using standard Fricke G-value dosimeters for Fe^{3+} = 15.5/100 eV of absorbed radiation energy. The dosimeter response was verified using a cobalt-60 radiation field (6 mm accumulation and 50 mm backscatter in a 300 mm × 300 mm collimated field). The output factor was determined using a tissue equivalent ionisation chamber calibrated in a standard NML field. During irradiation, the dose rate was 38.8 kGy/min, and the exposure times were calculated accordingly. The structural properties of the samples were examined by X-ray diffraction measurements using a Bruker D8 Advance diffractometer with a CuKα X-ray source of wavelength = 1.54 Å at 40 mA and 45 kV in the frequency range from 10° to 70°. The grazing incident θ;2θ method is used (Brentano Bragg configuration). The morphology of the films was characterised by scanning electron microscopy (SEM, Tescan Vega3 LMH) with the elemental mapping operated at a voltage of 20 kV, and by atomic force microscopy (AFM, DI-EnviroScope, Veeco). The principle of AFM consists of detecting the variations of deflections of a cantilever scanning the surface of a sample. These variations linked to the surface topography are measured using a laser beam reflected at the end of the cantilever and detected using photodiodes.

The chemical composition is characterised by X-ray photoelectron spectroscopy (XPS) using a VG Escalab 220I-XL system. The samples are placed in an ultra-high vacuum chamber of the spectrometer (vacuum of the order of 10^{-9} mbar) and irradiated by a monochromatic X-ray beam (Al Kα, 1.0 eV) with an energy hν of 1486.6 eV. Under this bombardment, core electrons are stripped off and collected by a 128-channel detector with a delay line system for spectroscopy and imaging and analysed by a 180° hemispherical analyser of 165 mm radius. A first measurement is performed, and then an ion etching is carried out (by Ar^+ ions) with an acceleration voltage of 2 kV for 3 minutes to avoid contamination of the analysed surface. The data are acquired using

Vision 2 Software and analysed using CasaXPS software to extract the components of the films. The energy correction of the spectra of the VO_2 samples is made with respect to the C1s peak of carbon placed at 285 eV.

3 Results and Discussions

Fig. 1(a) shows the X-ray diffraction pattern of the (VO_2) thin films deposited on a soda-lime glass substrate and subjected to the different irradiation doses (0, 50, 100 and 300 kGy). The patterns show peaks at 18.60, 27.83, 37.78, 40.07 and 57.8° [30]–[51] According to the Joint Committee on Powder Diffraction Standards (JCPDS No. 43-10-51), these peaks can be indexed as reflections from the (100), (011), (200), (020) and (022) planes, respectively. The prominent diffraction peaks of the four samples are the same, the only difference being in their intensities. This is clearly seen in Fig. 1(b) where the intensity values of the peaks associated with the (100) and (011) planes are plotted as a function of the irradiation dose.

The diffractograms shown in Fig. 1 indicate the exclusive presence of the monoclinic phase with the main orientation along the (100) plane, which corresponds closely to that of the monoclinic phase of (VO_2) (JCPDS No. 00-043-1051), with space group P21/c, and lattice parameters a = 5.75 Å, b = 4.54 Å, c = 5.38 Å, α = 90° and β = 122.60° [32]. Ngom *et al.* [12] reported on the crystal structure of vanadium dioxide (VO_2) nanostructures, showing a preferential orientation along the (100) direction. Synthesising (VO_2) thin films by pulsed laser ablation on a soda glass substrate under a pressure of 2.00 Pa, with a substrate cooling rate of 5 °C/min to 25 °C/min after vacuum deposition, they conclude that this main orientation along the (100) direction is due to the presence of a buffer layer of SiO_2 between the substrate and the (VO_2) thin films. Fig. 2 shows a decrease in the peak intensity for the (100) reflection plane when the gamma-ray irradiation dose increases from 0 to 50 kGy, followed by a monotonous increase from 100 to 300 kGy. A monotonous intensity decrease is observed for the (011) reflection plane. Fig. 3 shows the evolution of the crystallite size along the (100) and (011) reflection planes as a function of the irradiation dose. The crystallite size is determined from the diffraction *D* patterns (Fig. 1) on the surface of a sample using Debye Scherrer's equation:

$$D = \frac{0.94\lambda}{W\cos\theta} \quad (1)$$

Where *D* is the crystallite size, λ is the wavelength of the X-ray beam, W is the half-height width of the diffraction line (in radians) and θ is the diffraction angle [33]–[35].

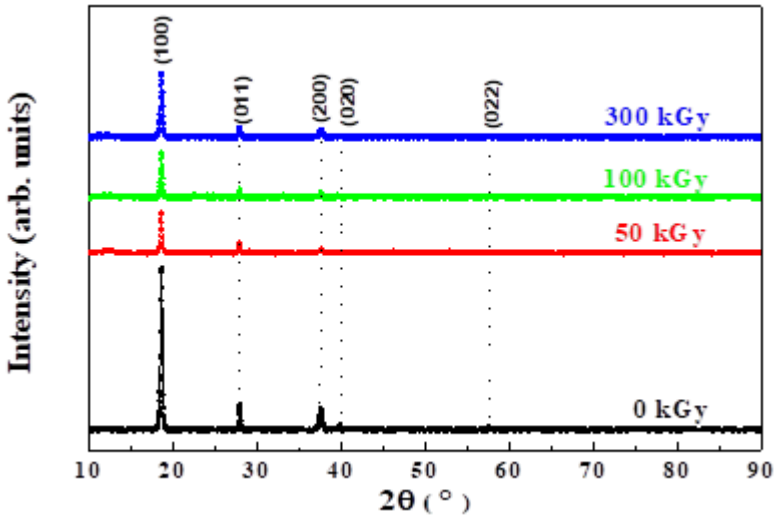

Fig. 1. XRD of the (VO_2) samples subjected to different radiation doses (0, 50, 100 and 300 kGy).

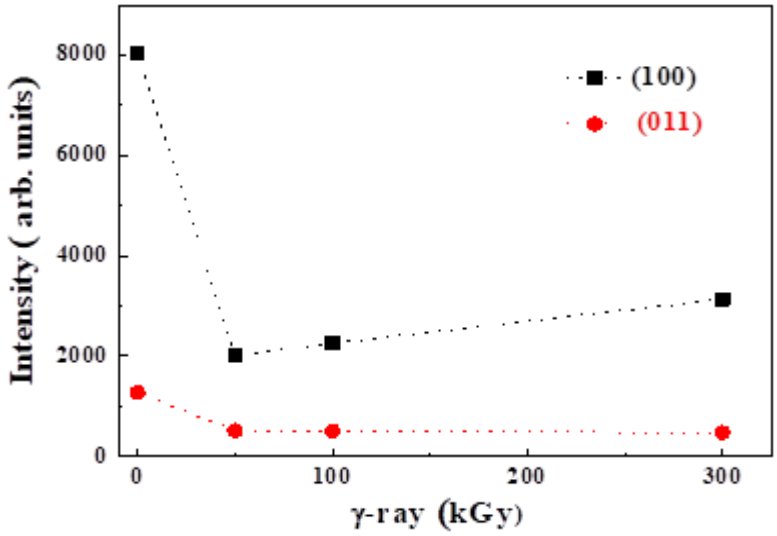

Fig. 2. Peak intensities of the (100) and (011 planes as function of the different radiation doses (0, 50, 100 and 300 kGy).

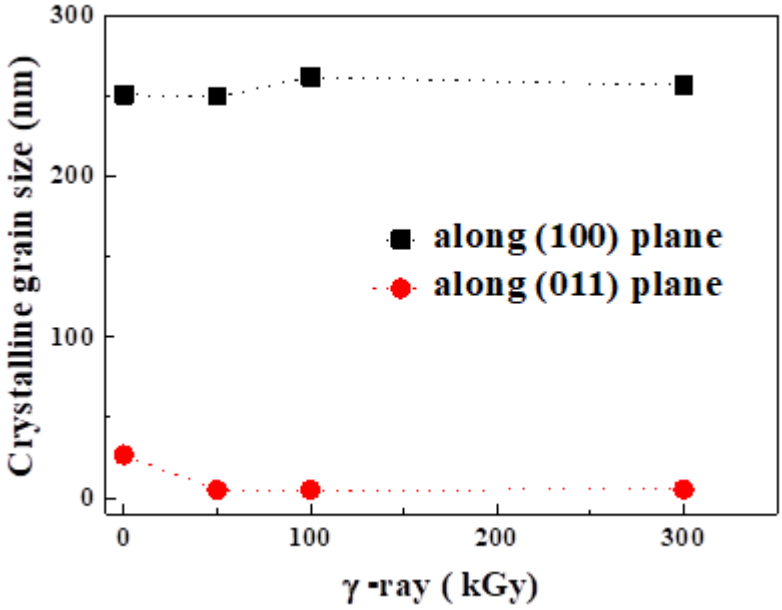

Fig. 3. Evolution of the crystallite size along the (100) and (011) reflection planes as a function of the irradiation dose.

The corresponding interplanar distances are also shown in Fig. 4 along the (100) and (011) reflection planes, respectively. The interplanar distances are determined by Bragg's law:

$$2d\sin\theta = n\lambda \qquad (2)$$

Where d is the interplanar distance, ie the distance between two crystallographic planes, θ is the half angle of deflection (half the angle between the incident and diffracted beam), n is the order of reflection (integer) and λ is the X-ray wavelength.

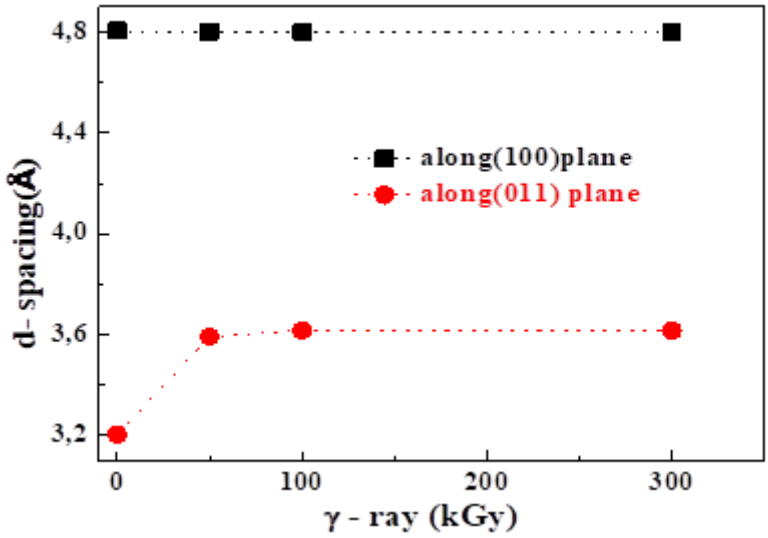

Fig. 4. Evolution of interplanar distance as a function of gamma radiation dose for the (100) and (011) plane.

Along the (100) reflection plane, the crystallite size does not show any regular trend. It first decreases at 50 kGy as compared to the plain sample, then it increases at 100 kGy and, finally, it decreases at 300 kGy. Along the (011) plane, a sharp decrease occurs at 50 kGy, followed by an almost constant value of the crystallite size beyond. The interplanar spacing of the plain sample corresponds to the (VO_2) monoclinic structure (JCPDS No. 43-1051). Along the (100) plane, it decreases as the dose increases from 0 to 100 kGy and it increases beyond 100 kGy. Along the (011) plane an increase is observed at 50 kGy as compared to the plain sample and then a plateau occurs. The proportion of vanadium valence states in deposited (VO_2) thin films subjected to different doses of gamma radiation was determined from XPS spectra. For this purpose, the sample was etched for 3 minutes before the measurements to remove contaminants from the vanadium oxide surface. The stripping time was established by monitoring the intensity decrease of the C1s peak of carbon, which is the main surface contaminant. Considering that the binding energy (BE) of the $V2p_{3/2}$ level depends on the oxidation state of the vanadium cation, the peak corresponding to this energy level was used to determine the proportion of valence states in the energy range from 512 ± 1 to 520 ± 1 eV, using the CasaXPS software and a Shirley-type function as a baseline. Fig. 5, 6, 7 and 8 show the vanadium ($V2p_{3/2}$ $(515.5 – 515.7) \pm 0.1$ eV and $V2p_{1/2}$ $(522.8 – 523.1) \pm 0.1$ eV) and oxygen ($(530.1 – 530.4) \pm 0.1$ eV) peaks which confirm the configurations of oxygen and the different vanadium ions (V^{3+}, V^{4+} and V^{5+}) of the (VO_2) thin films.

The XPS spectrum associated with the $V2p_{3/2}$ core level of the (VO_2) thin films was deconvolved in a combination of Gaussian/Lorentzian functions corresponding to the valence states V^{5+}, V^{4+} and V^{3+}. For the pristine sample, the peaks are positioned at BE = 516.4 ± 0.1 eV, 515.4 ± 0.1 eV and 514.4 ± 0.1 eV respectively (Fig. 5) [32]. BE shifts to 516.4 ± 0.1 eV, 515.4 ± 0.1 eV and 514.4 ± 0.1 eV (Fig. 6) [36] for an irradiation dose of 50 kGy, to BE = 516.4 ± 0.1 eV, 515.4 ± 0.1 eV and 514.3 ± 0.1 eV (Fig. 7) for the irradiation dose of 100 kGy and to BE = 516.5 ± 0.1 eV, 515.5 ± 0.1 eV and 514.5 ± 0.1 eV (Fig. 8) [37] for a dose of 300 kGy.

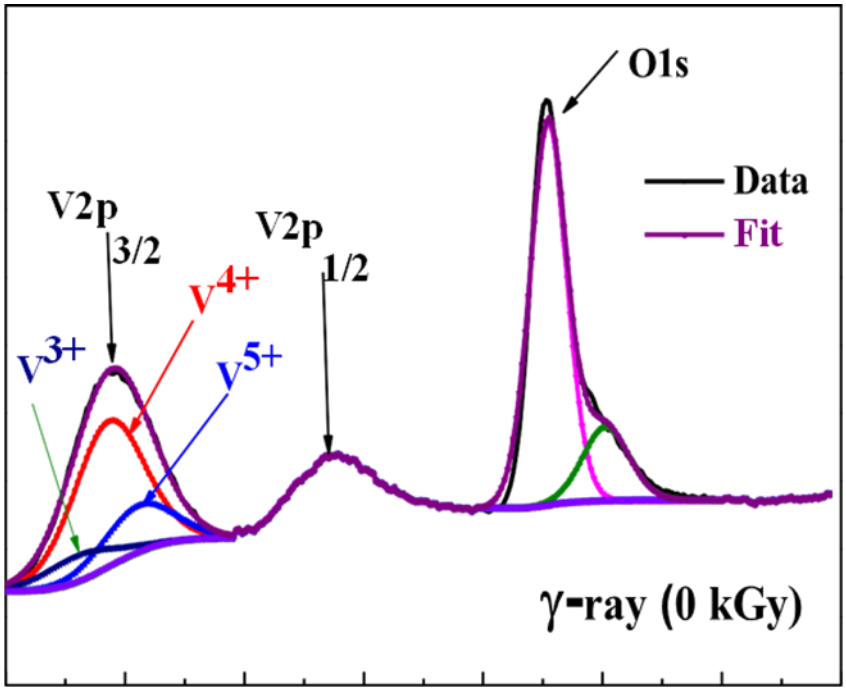

Fig. 5. XPS spectra of the $V2p_{3/2}$ decayed peak in three Gaussian/Lorentzian functions (V^{5+}, V^{4+} and V^{3+}) of the thin film deposited on the soda glass substrate subjected to a gamma radiation dose of 0 kGy.

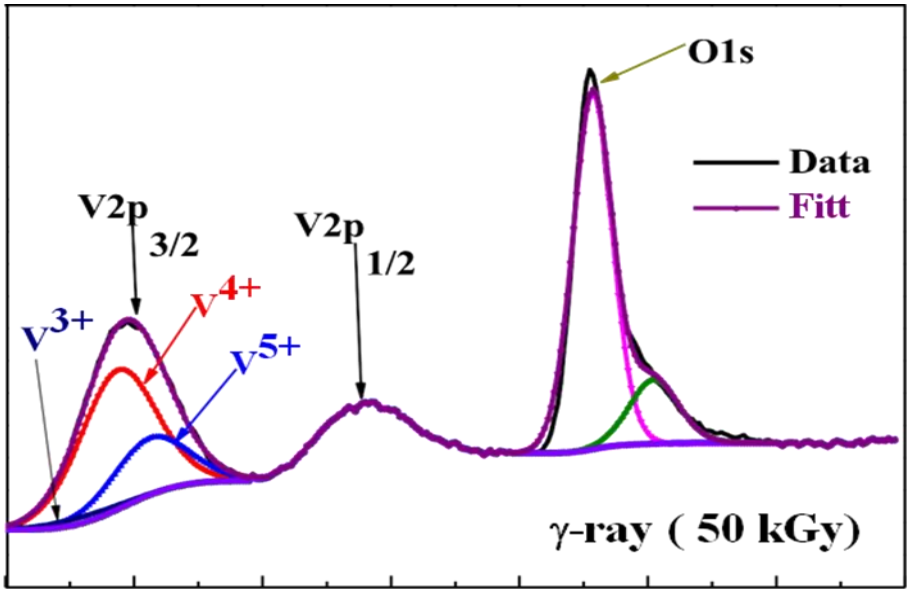

Fig. 6. XPS spectra of the $V2p_{3/2}$ decayed peak in three Gaussian/Lorentzian functions (V^{5+}, V^{4+} and V^{3+}) of the thin film deposited on the soda glass substrate subjected to a gamma radiation dose of 50 kGy.

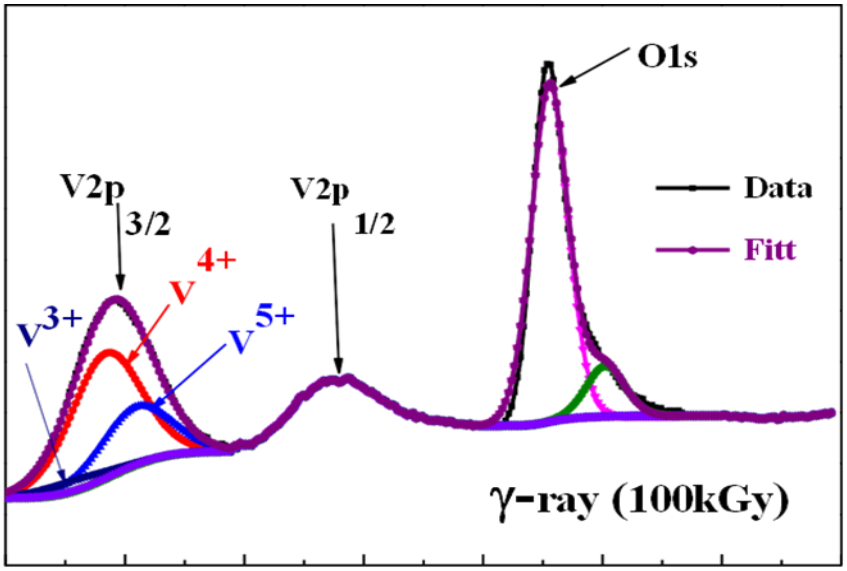

Fig. 7. XPS spectra of the $V2p_{3/2}$ decayed peak in three Gaussian/Lorentzian functions (V^{5+}, V^{4+} and V^{3+}) of the thin film deposited on the soda glass substrate subjected to a gamma radiation dose of 100 kGy.

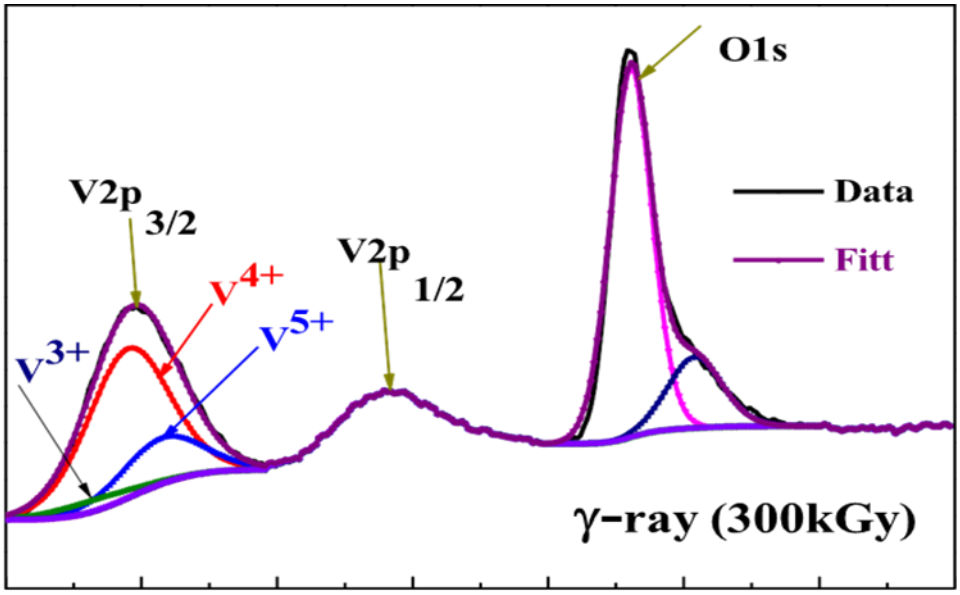

Fig. 8. XPS spectra of the $V2p_{3/2}$ decayed peak in three Gaussian/Lorentzian functions (V^{5+}, V^{4+} and V^{3+}) of the thin film deposited on the soda glass substrate subjected to a gamma radiation dose of 300 kGy.

The proportion of the various valence states of vanadium was calculated from the ratio of the areas under each of these three peaks. The four samples are mostly dominated by the V^{4+} valence state, which is characteristic of VO_2 (Fig. 9). In addition, the V^{5+} content increases when the dose varies from 0 to 50 kGy while the fraction of V^{3+} decreases. When thin films are bombarded by radiation, electrons can be removed from their orbit, causing oxidation of V^{3+} ions in (V_2O_3) because its electrons are less bound to the nucleus [38]. The variation of the irradiation dose from 50 to 100 kGy leads to an increase in the concentration of V^{3+} (V_2O_3) ions and a decrease in the concentration of V^{5+} (V_2O_5) ions. The effects of radiation on resistant materials generally consist of defect production, disorder and clustering, cluster growth, fragmentation, swelling and polygonisation [39], [40]. On the other hand, in materials that are more sensitive to damage accumulation, crystalline to crystalline phase transformations [41], [42], amorphisation [42], [43] and chemical effects (reduction of cations, loss of anions) [44], [45] are observed. For a thin film heated locally by gamma radiation, there is a deficit in oxygen and an increase in the concentration of V^{3+} ions [37]. A decrease in the density of the oxidation states V^{3+} and V^{5+}, and consequently an increase in the density of the valence state V^{4+} is observed for irradiation doses between 100 and 300 kGy, which favours the stability of vanadium dioxide (VO_2).

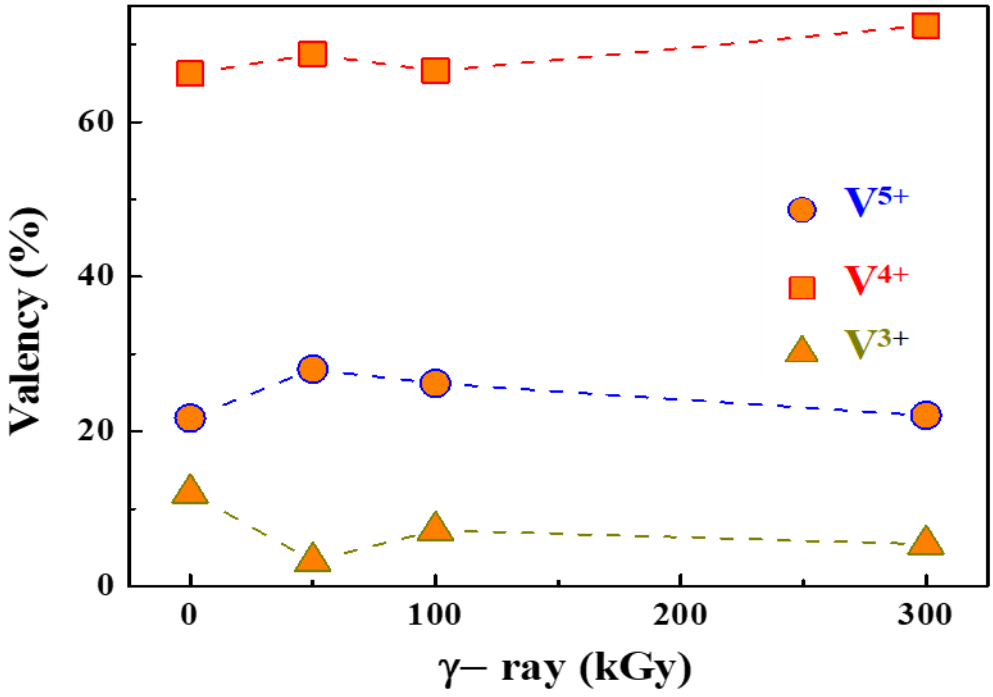

Fig. 9. Proportion of the valence states of vanadium valence state content in the thin films deposited on the soda glass substrates subjected to different gamma radiation doses from 0 to 300 kGy.

It has been reported that metal oxides undergoing irradiation undergo complex structural changes depending on the nature of the material, the energy of the radiation and the dose [46]. As (VO_2) is known to be thermodynamically stable and resistant to radiation, radiation doses up to 100 kGy are likely to induce defects, clustering, disorder and atomic displacements. However, some weakening of the crystal structure occurs at doses above 80 kGy [47]. Some XPS studies suggest that irradiation also affects the electronic structure of VO_2 with the reduction of the 3d band and a shift of the 2p band towards higher energies (higher valence cation state). This is the consequence of defects, gaps and atomic displacements. However, the stoichiometry of VO_2 is maintained [43]. Nevertheless, our results indicate a certain weakening of the crystallographic structure (XRD) at 50 kGy in the (100) plane as the main orientation. The XPS results indicate the presence of the 3 degrees of oxidation (V^{3+}, V^{4+} and V^{5+}) with an increase in irradiation up to 300 kGy favouring the formation of V^{4+}. Fig. 10(a–d) shows the AFM micrographs of the (VO_2) samples subjected to the different doses. There is a significant resemblance between the images.

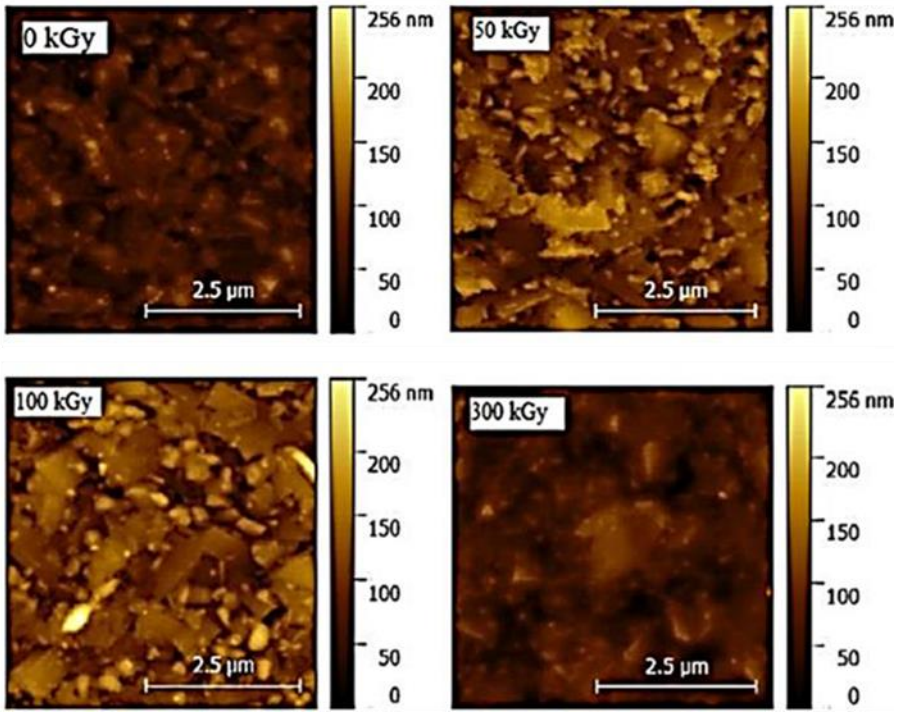

Fig. 10. (a)–(d) AFM images of the surface morphology of (VO_2) thin films subjected to 0 kGy, 50 kGy, 100 kGy and 300 kGy of gamma-ray irradiation doses, respectively.

All the samples are made of a mixture of grains of different sizes. The morphology is characterised by the presence of small grain sizes for the 50 and 100 kGy samples and large grain sizes for the 0 and 300 kGy samples. A statistical analysis of the results yields a mean grain size (dg) of 59.9 nm and RMS surface roughness (Rq) of 21.5 nm for pristine (VO_2) while dg = 95.4 nm and Rq = 28.3 nm for (VO_2) subjected to 50 kGy, dg = 108.4 nm and Rq = 26.4 nm at 100 kGy and finally dg = 94.1 nm and Rq = 21.4 nm at 300 kGy. In addition, the surface morphology of these thin layers differs significantly, as can be seen in the SEM images in Fig. 11. At the same time, small grains with a non-uniform distribution are present for samples subjected to gamma-ray irradiation of 0 and 300 kGy, larger grains with a much wider size distribution are present at 50 and 100 kGy. A correlation between the results obtained from the DRX, SEM and AFM analyses suggests that increasing gamma-ray irradiation first leads to an increase followed by a decrease in the crystallite size and surface roughness. The latter tends to return to its initial value as supported by SEM and AFM results, which means that the material regains its original morphology.

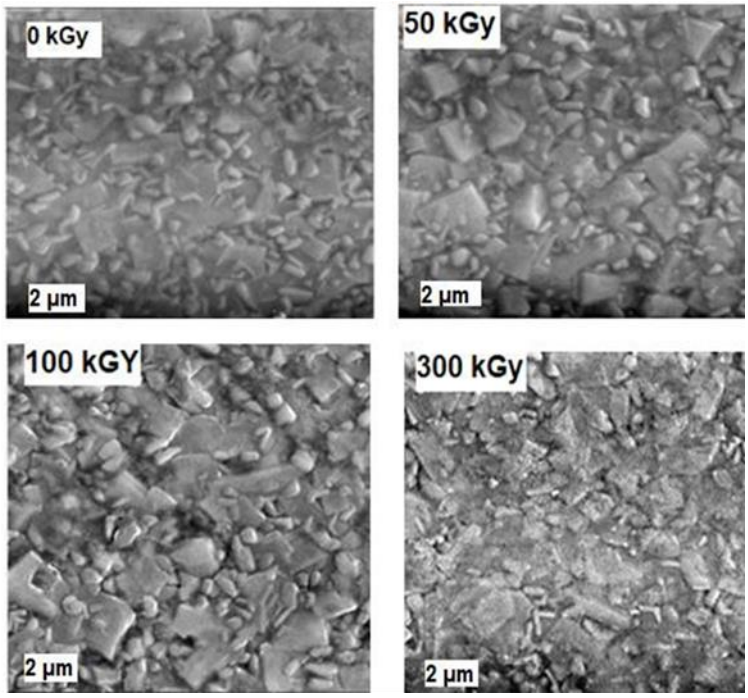

Fig. 11. SEM images (top view) of the VO_2 thin films subjected to 0 kGy, 50 kGy, 100 kGy and 300 kGy of gamma-ray radiation, respectively.

The resistivity variation during the heating and cooling cycles of the (VO_2) thin films subjected to different doses is shown in Fig. 12. The films show a first-order transition from the semiconducting to the metallic state, with an order of magnitude change in resistivity. Notable changes are observed in the transition temperature as the dose increases. The transition temperature (Fig. 13) increases linearly from 76.07 °C to 86.84 °C when the gamma ray dose increases from 0 kGy to 100 kGy. This increase in transition temperature can be induced by the grain size [48] and by the substrate temperature (600 °C) during deposition [49]. On the other hand, the transition temperature decreases from 86.84 °C to 75.03 °C, close to its initial value (76.07 °C) for doses ranging from 100 kGy to 300 kGy. In contrast, the hysteresis width (Fig. 14) follows the opposite trend. Overall, the electrical properties of the gamma-irradiated films show relatively modest changes that can be attributed to the creation of localised defect sites and some imperfections in the overall structure of the VO_2, leading to the observed broadening of the hysteresis width at higher dose [50].

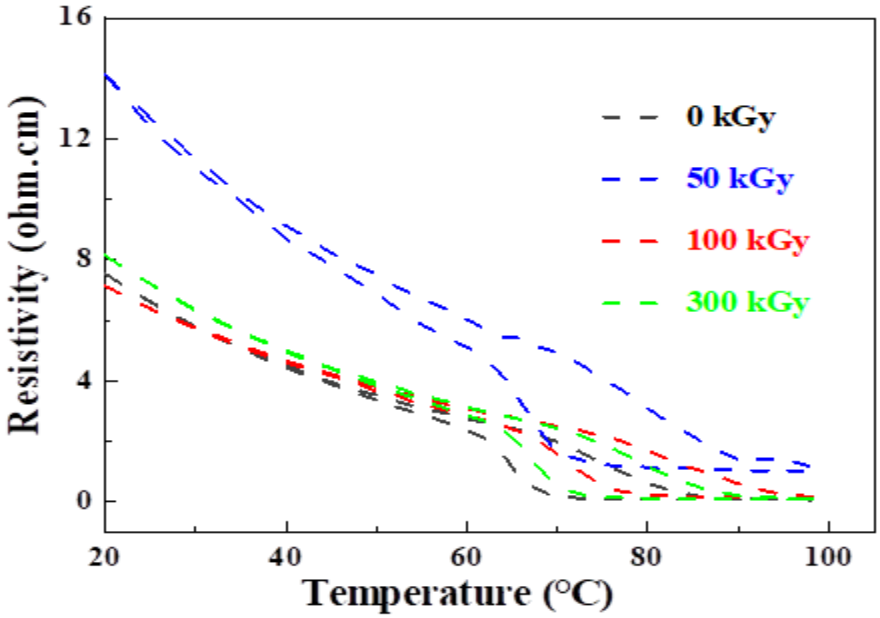

Fig. 12. Resistivity of VO_2 thin films deposited on soda glass substrates subjected to different gamma radiation dose as a function of temperature for heating and cooling.

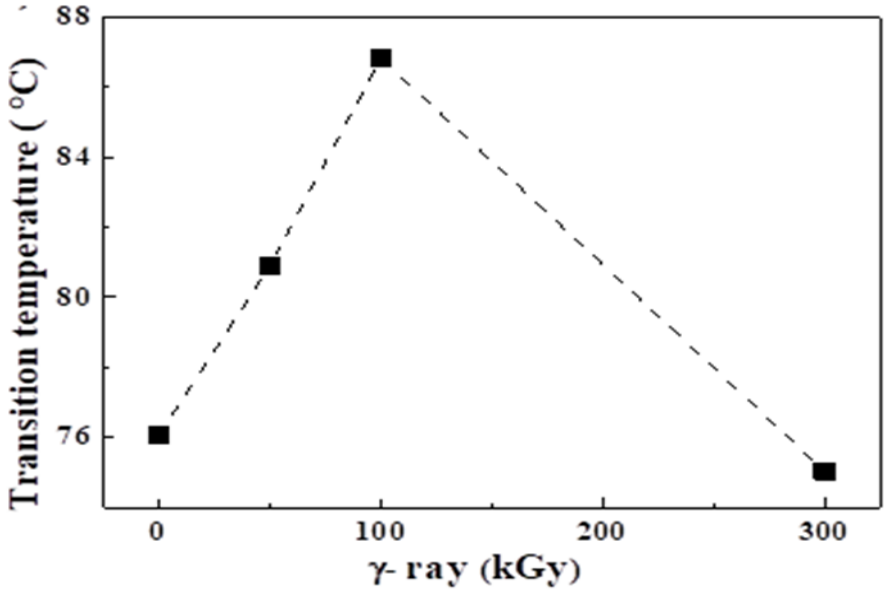

Fig. 13. Transition temperature as a function of gamma radiation dose.

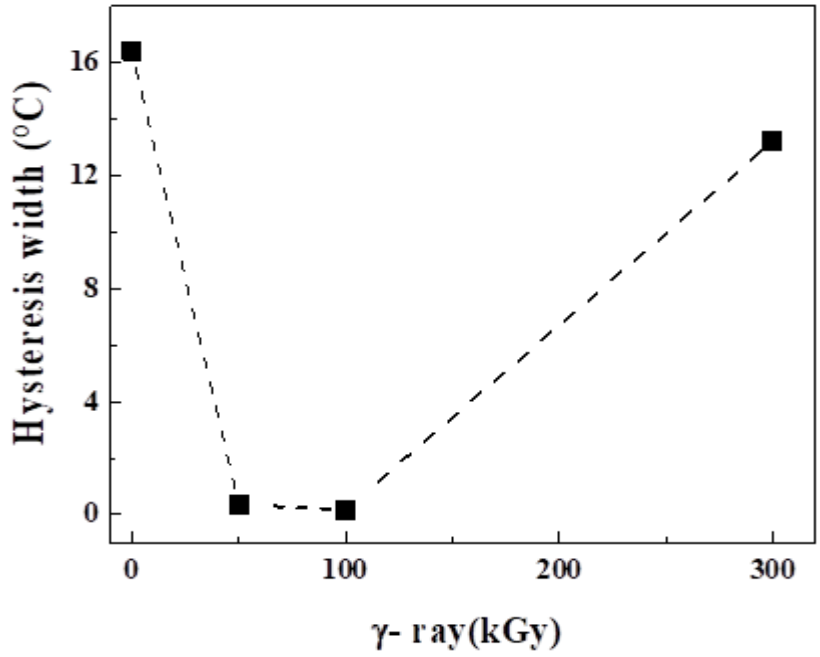

Fig. 14. Hysteresis as a function of gamma radiation dose.

4 Conclusions

We have shown that the crystal phase structure of VO_2 remains virtually intact during irradiation up to doses of 300 kGy. However, some weakening of the crystal structure occurs at doses of 50 kGy and 100 kGy. This is confirmed by XRD, which reveals that the crystallographic structure of VO_2 remains the same after gamma irradiation and still retains the same primary orientation (100). Irradiation also affects the electronic structure of VO_2 because studies (XPS) indicate that irradiation favours the formation of the V^{4+} (VO_2) state to the detriment of the V^{3+} (V_2O_3) and V^{5+} (V_2O_5) valence states. This is well supported by the study of morphological and electrical properties, which indicate that the electrical resistivity through the MIT is practically unaffected by gamma irradiation. We therefore believe that VO_2 films could be used advantageously for the thermal shielding of small spacecraft since their properties remain unchanged when subjected to gamma-ray doses such as those encountered during space missions.

5 Acknowledgments

This research was undertaken, in part, thanks to funding from the Canada Research Chairs Program. We thank Prof. Chaker for hosting this research at the National Institute for Scientific Research, Energy and Materials as the Canadian Chair holder.

6 References

[1] V. N. Andreev, and V. A. Klimov, "Electrical conductivity of the semiconducting phase in vanadium dioxide single crystals," *Phys. Solid State*, vol. 49, no. 12, pp. 2251–2255, 2007, doi: 10.1134/S1063783407120062.

[2] T.-H. Yang, R. Aggarwal, A. Gupta, H. Zhou, and R. J. Narayan, "Semi-conductor metal transition characteristics of VO_2 thin films grown on c- and r-sapphire substrates," *J. Appl. Phys.*, vol. 107, no. 5, pp. 053514–053514, 2010, doi: 10.1063/1.3327241.

[3] Y. Muraoka, and Z. Hiroi, "Metal-insulator transition of VO_2 thin films grown on TiO_2 (001) and (110) substrates," *J. Appl. Phys. Lett.*, vol. 80, no. 4, pp. 583–585, 2002, doi: 10.1063/1.1446215.

[4] J. I. Sohn *et al.*, "Stress-induced domain dynamics and phase transitions in epitaxially grown VO_2 nanowires," *J. Nanotechnol.*, vol. 23, no. 20, pp. 205–707, 2012, doi: 10.1088/0957-4484/23/20/205707.

[5] J. Y. Suh, R. Lopez, L. C. Feldman, and R. F. Haglund, "Semiconductor to metal phase transition in the nucleation and growth of VO_2 nanoparticles and thin films," *J. Appl. Phys.*, vol. 96, no. 2, pp. 1209–1213, 2004, doi: 10.1063/1.1762995.

[6] J. Cao *et al.*, "Strain engineering and one-dimensional organization of metal-insulator domains in single-crystal vanadium dioxide beams," *J. Nat. Nanotechnol.*, vol. 4, no. 11, pp. 732–737, 2009, doi: 10.1038/nnano.2009.266.

[7] J. Liu, Q. Li, T. Wang, D. Yu, and Y. Li, "Metastable vanadium dioxide nanobelts: Hydrothermal synthesis, electrical transport, and magnetic properties," *J. Angew. Chem.*, vol. 116, no. 38, pp. 5158–5162, 2004, doi: 10.1002/ange.200460104.

[8] T.-H. Yang, R. Aggarwal, A. Gupta, H. Zhou, R. J. Narayan, and J. Narayan, "Semiconductor metal, transition characteristics of VO_2 thin films grown on c- and r-sapphire substrates," *J. Appl. Phys.*, vol. 107, no. 5, p. 053514, 2010, doi: 10.1063/1.3327241.

[9] M. Soltani, M. Chaker, E. Haddad, R. V. Kruzelecky, and D. Nikanpour, "Optical switching of vanadium dioxide thin films deposited by reactive pulsed laser deposition," *J. Vac. Sci. Technol. Vac. Surf. Films*, vol. 22, no. 3, pp. 859–864, 2004, doi: 10.1116/1.1722506.

[10] A. Cavalleri, T. Dekorsy, H. W. Chong, J. C. Kieffer, and R. Schoenlein, "Evidence for a structurally-driven insulator-to-metal transition in VO_2: A view from the ultrafast timescale," *J. Phys. Rev. B*, vol. 70, no. 16, pp. 102–161, 2004, doi: 10.1103/PhysRevB.70.161102.

[11] Y. Ji *et al.*, "Role of microstructures on the M1-M2 phase transition in epitaxial VO_2 thin films," *J. Sci. Rep.*, vol. 25, pp. 48–54, 2014, doi: 10.1038/srep04854.

[12] B. D. Ngom *et al.*, "Competitive growth texture of pulsed laser deposited vanadium dioxide nanostructures on a glass substrate," *J. Acta Mater.*, vol. 64, no. 15, pp. 32–41, 2014, doi: 10.1016/j.actamat.2013.11.048.

[13] A. Hendaoui, N. Émond, M. Chaker, and E. Haddad, "Highly tunable-emittance-radiator based semiconductor-metal transition of VO_2 thin films," *J. Appl. Phys. Lett.*, vol. 102, p. 061107, 2013, doi: 10.1063/1.4792277.

[14] E. Haddad, R. V. Kruzelecky, B. Wong, W. Jamroz, and P. Poinas, *Large tuneability IR emittance thermal control coating for space applications*, 43rd Int. Conf Environ. Syst., AIAA, pp. 34–36, 2013, doi: 10.2514/6.2013-3436.

[15] B. L. Doyle, *Displacement Damage Caused by Gamma-rays and Neutrons on Au and Se*, SANDIA Report, 2014, doi: 10.2172/1177090.

[16] J. Kwon, and A. T. Motta, "Gamma displacement cross sections in various materials," *J. Ann. Nuc. Energy*, vol. 27, pp. 1627–1642, 2000, doi: 10.1016/S0306-4549(00)00024-4.

[17] G. H. Kinchin, and R. S. Pease, "The displacement of atoms in solids by radiation," *J. Rep. Prog. Phys.*, vol. 18, no. 1, pp. 1–51, 1955, doi: 10.1088/0034-4885/18/1/301.

[18] D. A. Thompson, "High density cascade effects," *Radiat. Eff.*, vol. 56, no. 3–4, pp. 105–150, 1981, doi: 10.1080/00337578108229885.

[19] A. G. Holmes-Siedle, and L. Adams, *Handbook of Radiation Effects*, Oxford: Oxford University Press, 1993.

[20] F. C. Case, "Modifications in the phase transition properties of redeposited VO_2 films," *J. Vac. Sci. Technol. A*, vol. 2, no. 4, pp. 1509–1512, 1984, doi: 10.1116/1.572462.

[21] F. C. Case, "Effects of low-energy low flux ion bombardment on the properties of VO_2 thin film," *J. Vac. Sci. Technol. A*, vol. 7, no. 3, pp. 1194–1198, 1989, doi: 10.1116/1.576252.

[22] A. Leone, A. M. Trione, and F. Junga, "Alteration in electrical and infrared switching properties of vanadium oxides due to proton irradiation," *IEEE Trans. Nucl, J. Sci*. vol. 37, no. 6, pp. 1739–1743, 1990, doi: 10.1109/23.101185.

[23] T. C. Lu, L. B. Lin, Q. Liu, Y. Lu, and X. D. Feng, “Reduction effects in rutile induced by neutron irradiation,” *Nucl. Inst. Methods J. Phys. Res. Sect. B*, vol. 191, no. 1–4, pp. 291–295, 2002.

[24] H. Karl, J. Peng, and B. Stritzker, “Effects of He-irradiation on the metal-to-insulator transition of vanadium dioxide nanoclusters,” *J. Mater. Res*., vol. 1256, pp. 12–56, 2010, doi: 10.1557/PROC-1256-N11-62.

[25] M. A. Nastasi, J. W. Mayer, and J. K. Hirvonen, *Ion-Solid Interactions: Fundamentals and Applications*, Cambridge: Cambridge University Press, 1996, doi: 10.1017/CBO9780511565007.

[26] R. A. Dugdale, and A. Green, “Some ordering effects in CusAu at about 100°,” *J. Philos. Mag.*, vol. 45, no. 361, pp. 1–63, 1954, doi: 10.1080/14786440208520435.

[27] Z. Li, *Radiation damage effects in Si materials and detectors and rad-hard Si detectors for SLHC*, IOP of science, Pixel 2008 int. workshop, Fermilab, Botavia, IL, USA, 2008.

[28] J. W. Cleland, J. H. Crawford, K. Lark Horovitz, J. C. Pigg, and F. W. Young, “The effect of fast neutron bombardment on the electrical properties of Germanium,” *J. Phys. Rev.*, vol. 8, no. 2, pp. 312–319, 1951, doi: 10.1103/PhysRev.83.312.

[29] R. Stoenescu, “Effects of neutron irradiation on the microstructure and mechanical properties of the heat affected zone of stainless-steel welds,” PhD thesis, EPFL, Lausanne, Switzerland, 2005.

[30] V. Eyert, “The metal-insulator transitions in VO_2: A band theoretical approach,” *J. Ann. Phys.*, vol. 514, no. 9, pp. 650–702, 2002, doi: 10.1002/1521-3889(200210)11:9<650::AID-ANDP650>3.0.CO;2-K.

[31] M. Chandrasekar *et al.*, “Specific charge separation of Sn- doped MgO nanoparticles for photocatalytic activity under UV light irradiation,” *J. Sep. Pur. Tech.*, vol, 294, p. 121189, 2022, doi: 10.1016/j.seppur.2022.121189.

[32] G. Garry, O. Durand, and A. Lordereau, ‘Structural, electrical and optical properties of pulsed laser deposited VO_2 thin films on R- and C-sapphire planes,” *Thin Solid Films*, pp. 453–427, 2004, doi: 10.1016/j.tsf.2003.11.118.

[33] V. Perumal *et al.*, “Enhancement of surface photocatalytic performance—Hierarchical SnO nanorods treated against methylene blue dye under solar irradiation and biological degradation,” *J. Env. Res.*, vol. 209, p. 112821, 2022, doi: 10.1016/j.envres.2022.112821.

[34] V. Perumal *et al.*, “SnO decorated hierarchical graphene oxide nanotiges with high photocatalytic performance for energy conversion applications,” *J. Fuel.*, vol. 324, p. 124599, 2022, doi: 10.1016/j.fuel.2022.124599.

[35] S. Panimalar *et al.*, “Reproducibility and long-term stability of Sn-doped MnO nanostructures: practical photocatalytic systems and wastewater treatment applications,” *J. Chem.*, vol. 293, p. 133646, 2022, doi: 10.1016/j.chemosphere.2022.133646.

[36] T.-W. Chiu, K. Tonooka, and N. Kikuchi, “Influence of oxygen pressure on the structural, electrical and optical properties of VO_2 thin films deposited on ZnO/glass substrates by pulsed laser deposition,” *J. Thin Solid Films*, vol. 518, no. 24, pp. 7441–7444, 2010, doi: 10.1016/j.tsf.2010.05.019.

[37] E. Hryha, E. Rutqvist, and L. Nyborg, “Stoichiometric vanadium oxides studied by XPS,” *J. Surf. Interface. Anal.*, vol. 44, pp. 10–22, 2012, doi: 10.1002/sia.3844.

[38] A. G. Holmes-Siedle, and L. Adams, *Handbook of Radiation Effects*, Oxford: Oxford University Press, 1993.

[39] C. L. Tracy, J. McLain Pray, M. Lang, D. Popov, C. Park, and C. Trautmann, “Defect accumulation in THO_2 irradiated with swift heavy ions,” *J. Nucl, Instrum. Meth.*, vol. 326, pp. 169–173, 2014, doi: 10.1016/j.nimb.2013.08.070.

[40] T. Wiss, H. Matzke, C. Trautmann, M. Toulemonde, and S. Klaumunzer, “Radiation damage in UO_2 by swift heavy ions,” *J. Nucl. Instrum. Meth.*, vol. 122, no. 3, pp. 583–588, 1997, doi: 10.1016/S0168-583X(96)00754-9.

[41] A. Benyagoub, “Mechanism of the monoclinic-to-tetragonal phase transition induced in zirconia and hafnia by swift heavy ions,” *J. Phys. Rev.*, vol. 72. P. 094114, 2005, doi: 10.1103/PhysRevB.72.094114.

[42] M. Lang *et al.*, “Swift heavy ion-induced phase transformation in Gd_2O_3,” *Nucl. Instrum. Meth.*, vol. 326, pp. 121–125, 2014, doi: 10.1016/j.nimb.2013.10.073.

[43] W. Weber, “Models and mechanisms of irradiation-induced amorphization in ceramics,” *Nucl. Instrum. Meth.*, vol. 167, pp. 98–106, 2000, doi: 10.1016/S0168-583X(99)00643-6.

[44] V. Saikiran, N. Srinivasa Rao, G. Devaraju, G. S. Chang, and P. Pathak, “Ion beam irradiation effects on Ge nanocrystals synthesized by using RF sputtering followed by RTA,” *Nucl. Instrum. Meth.*, vol. 312, pp. 161–164, 2013, doi: 10.1016/j.nimb.2013.04.008.

[45] S. Takaki, K. Yasuda, T. Yamamoto, S. Matsumura, and N. Ishikawa, “Atomic structure of ion tracks in Ceria,” *Nucl. Instrum. Meth.*, vol. 326, pp. 140–144, 2014, doi: 10.1016/j.nimb.2013.10.077.

[46] A. Gupta, R. Singhal, J. Narayan, and D. K. Avasthi, “Electronic excitation induced controlled modification of semiconductor-to-metal transition in epitaxial VO_2 thin films,” *J. Mater. Res.*, vol. 26, pp. 2901–2906, 2011, doi: 10.1557/jmr.2011.392.

[47] I. G. Madiba, N. Émonde, M. Chaker, and F. T. Thema, “Effects of gamma irradiations on reactive pulsed laser deposited vanadium dioxide thin films,” *J. Appl Surf Science*., vol. 411, pp. 271–278, 2017, doi: 10.1016/j.apsusc.2017.03.131.

[48] J. Suh, R. Lopez, L. C. Feldman, and R. F. Haglung, “Semiconductor to metal phase transition in the nucleation and growth of VO_2 nanoparticles and thin film,” *J. Appl. Phys.*, vol. 96, p. 1209, 2004, doi: 10.1063/1.1762995.

[49] J. B. Kana *et al.*, “Thermochromic VO_2 thin films synthesized by inverted cylindrical magnetron sputtering,” *J. Appl. Surf. Sci.*, vol. 234, no. 13, pp. 3959–3963, 2008, doi: 10.1016/j.apsusc.2007.12.021.

[50] L. Hongwei *et al.*, “Size effects on metal-insulator phase transition in individual vanadium dioxide nanowires,” *J. Opt. Express*, vol. 22, pp. 30748–30755, 2014, doi: 10.1364/OE.22.030748.

[51] M. Subash *et al.*, “Pseudo-kinetic model of copper doping on the structural, magnetic and photocatalytic activity of magnesium oxide nanoparticles for energy application,” *J. Bio. Conv. Bior.*, vol. 13, pp. 3427–3437, 2023, doi: 10.1007/s13399-022-02993-1.